

# Efficient time-series prediction on NISQ devices via time-delayed quantum extreme learning machine

Mio Kawanabe,<sup>1</sup> Saud Ćindrak,<sup>2</sup> Kathy Ludge,<sup>2</sup> Jun-ichi Shirakashi,<sup>1,\*</sup> Tetsuo Shibuya,<sup>3</sup> and Hiroshi Imai<sup>4</sup>

<sup>1</sup>*Department of Electrical Engineering and Computer Science,  
Tokyo University of Agriculture and Technology, Koganei, Tokyo 184-8588, Japan*

<sup>2</sup>*Institute of Physics, Technische Universitat Ilmenau, Ilmenau, Germany*

<sup>3</sup>*Division of Medical Data Informatics, Human Genome Center,  
The Institute of Medical Science, The University of Tokyo, Minato, Tokyo 108-8639, Japan*

<sup>4</sup>*The Graduate School of Information Science and Technology,  
The University of Tokyo, Bunkyo, Tokyo 113-8656, Japan*

(Dated: February 26, 2026)

We proposed a time-delayed quantum extreme learning machine (TD-QELM) for efficient time-series prediction on noisy intermediate-scale quantum (NISQ) devices. By encoding multiple past inputs simultaneously, TD-QELM achieves shallow circuit depth independent of sequence length, thereby, mitigating noise accumulation and reducing computational complexity. Experiments using the NARMA benchmark on both noiseless simulations and IBM’s 127-qubit processor demonstrate that TD-QELM consistently outperforms conventional quantum reservoir computing in prediction accuracy and noise robustness. These results highlight TD-QELM as a practical and scalable framework for time-series learning on current NISQ hardware.

*Introduction.* In recent years, quantum computing has emerged as a transformative technology with the potential to revolutionize a wide range of scientific and engineering disciplines [1]. However, current quantum computers remain limited by noise originating from imperfections in quantum hardware, placing them in the era of noisy intermediate-scale quantum (NISQ) devices [2, 3]. Quantum algorithms that promise computational advantage typically require millions of qubits and deep circuits, rendering them impractical for near-term devices.

Among the various approaches compatible with NISQ hardware, *quantum machine learning* (QML) has emerged as a promising and robust framework [4–7]. QML explores how machine learning algorithms can be efficiently implemented using quantum systems. Within this field, *quantum reservoir computing* (QRC) employs quantum systems as dynamical reservoirs in which only the readout layer is trained [8]. This approach has attracted significant attention, particularly in the domains of time-series forecasting and nonlinear dynamical modeling [9–19]. Recent research show cases that optimal performance is achieved at dynamical phase transitions [20] and at the edge of quantum chaos [21]. Furthermore, [22, 23] introduced a measure based on Krylov complexity, showing near-perfect correlations with data expressivity in QRC, thus linking computational performance with insights into complex quantum systems.

Although noise is often detrimental in quantum algorithms, specific types of noise have been shown to enhance computational performance in QRC [9, 10, 24–29]. For instance, dissipative QRC has been shown to outperform noiseless implementations [9, 25, 26, 29]. In a similar vein, Suzuki et al. demonstrated that the in-

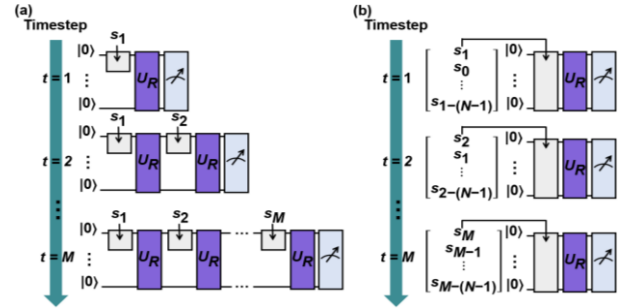


FIG. 1. Conceptual Diagrams of QRC and TD-QELM. (a) In the restarting protocol, input encoding and unitary evolution  $U_R$  are sequentially applied at each timestep to incorporate past information. This causes circuit depth and computational cost to grow quadratically with sequence length  $M$ . (b) The current input  $s_t$  and  $N - 1$  time-delayed inputs  $s_t, s_{t-1}, \dots, s_{t-(N-1)}$  are simultaneously encoded into  $N$  qubits, keeping the circuit shallow regardless of  $M$ .

trinsic noise inherent to superconducting quantum processors can enhance performance in time-series learning tasks [10].

Despite these advantages, QRC faces a fundamental challenge when applied to sequential data. Each measurement collapses the quantum state, leading to a loss of quantum information [8]. Reconstructing the system state therefore requires re-initializing the entire time series up to the current step, resulting in increasing computational overhead and circuit depth [30–34]. In noisy circuits, this results in noise accumulation, which further degrades performance. Several strategies have been proposed to mitigate these limitations. Mujal *et al.* employed weak measurements, while Ćindrak *et al.* exploited the fading-memory property of the reservoir to periodically reset the system [30, 33]. Other studies have introduced feedback mechanisms or auxiliary qubits to

\* shrakash@cc.tuat.ac.jp

counteract state collapse [31, 34, 35]. Although these techniques improve practicality, QRC still relies on sequential processing, handling one timestep at a time.

To address these challenges, we propose the *Time-Delayed Quantum Extreme Learning Machine* (TD-QELM), inspired by the classical *Time-Delayed Extreme Learning Machine* (TD-ELM) [36]. TD-QELM mitigates the issues of circuit depth and computational cost by considering only a subset of past inputs and enabling parallelized input encoding, similar to previous works [15, 30, 37, 38]. This design yields quantum circuits whose depth is independent of the input sequence length, thereby suppressing noise accumulation and reducing computational complexity from quadratic to linear order. The authors of [39] provided evidence that QELM architectures built from random circuits exhibit strong concentration effects, which severely limit their learning capability. To avoid these issues, our approach employs the transverse-field Ising model as a structured reservoir in the noiseless simulation. We then implement this reservoir via a one-step Trotterization of a 6-qubit model, resulting in shallow quantum circuits on IBM’s 127-qubit superconducting processor *ibm.kawasaki* as well as its corresponding simulator *FakeKawasaki* [40].

The effectiveness of TD-QELM is evaluated using the Nonlinear AutoRegressive Moving Average (NARMA) benchmark for time-series forecasting. Our results show that TD-QELM consistently outperforms the standard QRC protocol across different noise conditions. In particular, TD-QELM maintains stable performance for longer input sequences, whereas QRC performance deteriorates due to increasing noise accumulation. These results indicate that TD-QELM enables more robust and resource-efficient time-series forecasting on current NISQ devices.

*Quantum reservoir computing.* Quantum Reservoir Computing (QRC) aims to leverage the large Hilbert space of a quantum system to perform time-series prediction tasks [8]. The system is described by a Hamiltonian  $H$  and its corresponding unitary operator  $U_R = \exp(-iHT)$  for some  $T > 0$ . The approach typically works by first encoding the current input  $s_t$  of a time series  $(s_t)_t$  into one of the qubits via

$$|\psi_{\text{in}}(s_t)\rangle = \sqrt{1-s_t} |0\rangle + \sqrt{s_t} |1\rangle, \quad (1)$$

which is applied to the first qubit. The full system state is then given by

$$\rho_{\text{in}}(s_t) = |\psi_{\text{in}}(s_t)\rangle \langle \psi_{\text{in}}(s_t)| \otimes \text{Tr}_1(\rho(s_{t-1})), \quad (2)$$

where  $\rho(s_{t-1})$  denotes the system state before encoding. After evolution under the reservoir  $U_R$ , the system state becomes

$$\rho(s_t) = U_R \rho_{\text{in}}(s_t) U_R^\dagger. \quad (3)$$

In QRC, expectation values of the observables  $\{\sigma_z^{(k)}\}_{k=1,\dots,K}$  define the reservoir output features and are given by  $x_{t,k} = \text{Tr}(\sigma_z^{(k)} \rho(s_t))$ . They form the

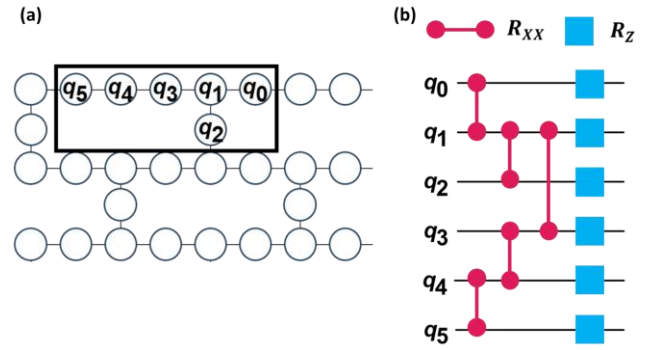


FIG. 2. (a) Connectivity map of the qubits used in the experiment within the *ibm.kawasaki* device topology (partially shown), where each  $q_i$  represents a qubit. The connections define a hardware-specific topology  $E$ . (b) Hardware-efficient circuit using Trotterization, designed to implement a multi-qubit quantum system under real-device connectivity constraints. This design reduces gate operations while maintaining sufficient entanglement on NISQ hardware.

state matrix  $X_{t,k} = x_{t,k}$  with  $X \in \mathbb{R}^{T,K}$  and  $\mathbf{x}_t = (x_{t,1}, \dots, x_{t,K})$ . To increase the readout dimension, time-multiplexing at  $N_V$  times  $\tau_n = nT/N_V$  with  $n \in \{1, 2, \dots, N_V\}$  is employed, resulting in a total of  $N_R = KN_V$  expectation values per input. The predicted output is then given by

$$y_t = \mathbf{x}_t \mathbf{w}_{\text{out}}, \quad (4)$$

where the readout weights  $\mathbf{w}_{\text{out}}$  are optimized to minimize the loss  $L = (\mathbf{y} - \hat{\mathbf{y}})^2$ , and are obtained as

$$\mathbf{w}_{\text{out}} = (X^\top X)^{-1} X^\top \hat{\mathbf{y}}, \quad (5)$$

where  $\hat{\mathbf{y}}$  is the desired target vector. A finite number of measurements introduces shot noise proportional to  $1/\sqrt{N_{\text{shots}}}$ , which acts both as a limiting factor and as an effective regularizer [30].

Since the quantum state collapses after each measurement, the system must be fully reinitialized at every input of the time series (see Fig. 1(a)). The  $s_n$ -th input therefore requires  $n_{\text{enc}} = n$  encodings and  $n_R = n$  reservoir evolutions. The computational cost of QRC for a time series of length  $M$  is

$$T_{\text{QRC}} = \sum_{n=1}^M n = \frac{M(M+1)}{2} \in \mathcal{O}(M^2), \quad (6)$$

demonstrating quadratic scaling [8, 30].

*Time-Delayed QELM.* To address the need for reinitializing the full time series, we propose a Quantum Extreme Learning Machine approach for time-series prediction, termed **TD-QELM** (see Fig. 1(b)). In TD-QELM, the system is initialized in the state  $|\psi_{\text{init}}\rangle = |00\dots 0\rangle$  for each input  $s_t$ . As input to the TD-QELM, we consider a vector of  $N$  previous inputs,  $\mathbf{s}_t = (s_{t-\tau_1}, s_{t-\tau_2}, \dots, s_{t-\tau_N})$ . After encoding, the resulting state is  $|\psi_{\text{in},t}\rangle = U_E(\mathbf{s}_t) |\psi_{\text{init}}\rangle$ . In this work, each

component of  $\mathbf{s}_t$  is encoded into a separate qubit following Eq. (1). After evolution under  $U_R$ , the output state and density matrix are given by

$$|\psi(s_t)\rangle = U_R |\psi_{\text{in},t}\rangle, \quad \rho(s_t) = |\psi(s_t)\rangle \langle \psi(s_t)|. \quad (7)$$

Given that the number of qubits is  $N$ , this approach requires only  $n_{\text{enc}} = 1$  encoding of the input vector  $\mathbf{s}_t$  and  $n_R = 1$  reservoir evolution  $U_R$ . The computational cost for TD-QELM is therefore

$$T_{\text{TD-QELM}} = \sum_{n=1}^M 1 = M \in \mathcal{O}(M), \quad (8)$$

showing linear complexity with respect to the length of the time series.

A standard benchmark for testing both the nonlinearity and memory capacity of a reservoir is the NARMA10 time-series prediction task, which is defined as

$$y_{t+1} = 0.3y_t + 0.05y_t \sum_{d=0}^9 y_{t-d} + 1.5s_t s_{t-9} + 0.1, \quad (9)$$

where  $s_t$  is uniformly distributed in  $[0, 0.2]$ . The time-step  $t$  input-encoding we employ for the TD-QELM is defined as

$$|\psi_{\text{in},t}\rangle = |\psi(s_t)\rangle \otimes |\psi(s_{t-1})\rangle \otimes |\psi(s_{t-2})\rangle \\ \otimes |\psi(s_{t-9})\rangle \otimes |\psi(s_{t-10})\rangle \otimes |\psi(s_{t-11})\rangle, \quad (10)$$

which follows the information processing capacity analysis of Kubota [41, 42]. Such delayed input encoding has been shown to significantly increase task performance in classical reservoir computing [43–45]. The target at time-step  $t$  is given by  $y_{t+1}$  according to Eq. (9). As a performance metric, we compute the signal Normalized Mean Squared Error (NMSE), as commonly used in quantum reservoir computing (QRC) [11], where  $\mathbf{y} = (y_1, \dots, y_T)$  and  $\mathbf{y}^{\text{target}} = (y_1^{\text{target}}, \dots, y_T^{\text{target}})$  denote the output and target signals, with  $y_t^{\text{target}} = y_{t+1}$  (Eq. (9)), which is defined as

$$\text{NMSE} = \frac{\sum_{t=1}^T (y_t - y_t^{\text{target}})^2}{\sum_{t=1}^T (y_t^{\text{target}})^2}. \quad (11)$$

TABLE I. NMSE of TD-QELM and QRC for the NARMA10 task with varying readout dimension  $N_R = N_V N_S$ . The results of a linear regression model (LR) with readout dimension are shown for comparison. Boldface indicates the best NMSE for each readout dimension. Results are computed on a time series of length  $M = 5000$ , with 10% used for washout, 70% for training, and 20% for testing.

Readout dim. $N_R$	TD-QELM NMSE	QRC NMSE	LR NMSE
30	$9.83 \cdot 10^{-4}$	$3.33 \cdot 10^{-3}$	<b><math>7.47 \cdot 10^{-4}</math></b>
60	<b><math>4.55 \cdot 10^{-4}</math></b>	$2.73 \cdot 10^{-3}$	$7.38 \cdot 10^{-4}$
120	<b><math>3.08 \cdot 10^{-4}</math></b>	$2.06 \cdot 10^{-3}$	$7.58 \cdot 10^{-4}$
300	<b><math>2.68 \cdot 10^{-4}</math></b>	$1.85 \cdot 10^{-3}$	$8.34 \cdot 10^{-4}$
600	<b><math>2.73 \cdot 10^{-4}</math></b>	$1.59 \cdot 10^{-3}$	$1.04 \cdot 10^{-3}$

For comparison, in machine learning one typically employs a variance-normalized error measure  $\text{NMSE}_{\text{var}} = \sum_{t=1}^T (y_t - y_t^{\text{target}})^2 / \sum_{t=1}^T (y_t - \mathbb{E}[\mathbf{y}])^2$ , where  $\mathbb{E}[\mathbf{y}] = T^{-1} \sum_{t=1}^T y_t$  denotes the expectation value of the target signal. The two errors are related as follows (see App. A for the derivation):  $\text{NMSE}_{\text{var}} = \text{NMSE} \left(1 + \frac{\mathbb{E}[\mathbf{y}]^2}{\text{var}[\mathbf{y}]}\right)$ .

To test **TD-QELM**, we compare this method against standard **QRC** practices. The most commonly used quantum reservoir in QRC is the *transverse-field Ising model*, given by

$$H = \sum_{i,j \in E} J_{i,j} \sigma_x^{(i)} \sigma_x^{(j)} + h \sum_i \sigma_z^{(i)}, \quad (12)$$

where  $J_{i,j}$  are sampled uniformly from the interval  $[-5, 5]$  and the external field is set to  $h = 5$ . For a statistical analysis, we consider ten realizations of such reservoirs with random  $J_{i,j}$  and plot the averaged performance. For the theoretical simulations, we allow interactions between all qubits, i.e., the connectivity matrix is  $E_1 = \{(i, j) \mid i, j \in \{0, \dots, N_S - 1\}\}$ , where  $N_S = 6$  is the number of qubits. To implement quantum reservoirs on actual hardware, and considering that the current generation of **NISQ** devices cannot support large circuit depths, we employ a simple one-step Trotterization, as illustrated schematically in Fig. 2(b) [3]. This results in the unitary circuit

$$U(\boldsymbol{\theta}) = \left( \prod_{i=0}^{N_S} R_Z^{(i)}(2h) \right) \left( \prod_{i,j=0}^{N_S} R_{XX}^{(i,j)}(2J_{i,j}) \right) \quad (13)$$

proposed by Kandala *et al.* [29, 46, 47]. Simulations of both **TD-QELM** and **QRC** with connectivity  $E_1$  were performed using the `aer_simulator_density_matrix` backend in **IBM Qiskit**.

We then consider a quantum hardware platform with restricted qubit coupling topology, given by  $E_2 = \{(0, 1), (1, 2), (1, 3), (3, 4), (4, 5)\}$ . These circuits are implemented on the 127-qubit NISQ device *ibm.kawasaki* (see Fig. 2(a)), and a corresponding backend simulation **FakeKawasaki** is also performed.

*Results.* Table I summarizes the NMSE for TD-QELM, QRC, and a linear model (LR). For TD-QELM and QRC, the NMSE values are averaged over 10 quantum systems. We use a 1-step Trotter circuit and measure the six sites in the Pauli- $z$  direction, given by  $\sigma_z^{(i)}$ , a total of  $N_V \in \{5, 10, 20, 50, 100\}$  times. For comparison, we consider the last  $N_R$  inputs,  $\mathbf{x}_t = (s_t, s_{t-1}, \dots, s_{t-N_R+1})$ , as the system state and construct a linear regression (LR) model. Training is performed in the same manner. We use  $M = 5000$  data points in total, allocating 10% for washout, 70% for training, and 20% for testing.

With a small readout dimension ( $N_R = 30$ ), the best-performing model is the linear model (LR), which successfully captures the required memory aspects of the NARMA10 task. However, increasing the readout dimension allows the TD-QELM to sample more

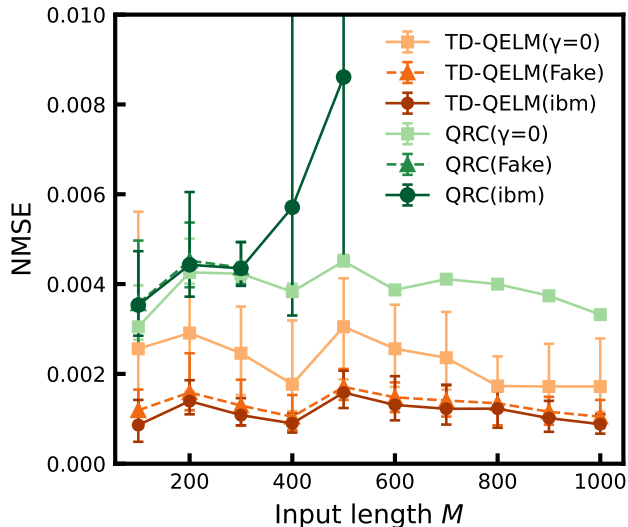


FIG. 3. Average NMSE of TD-QELM and QRC as a function of input length  $M$  under ideal noiseless simulation ( $\gamma = 0$ ), a hardware-mimicking noise model (**FakeKawasaki**, denoted as “Fake” in the legend), and a real NISQ device (*ibm.kawasaki*, denoted as “ibm”), using 10% washout, 70% training, and 20% testing.  $N_S = 6$  sites are considered with  $N_V = 1$  multiplexing. TD-QELM maintains low NMSE even for long input sequences, whereas QRC shows rapid performance degradation. Error bars indicate the range between the maximum and minimum values over 10 trials.

effectively from the large Hilbert space, thereby improving task performance and achieving an error of  $\text{NMSE}(\text{TD-QELM}) = 2.73 \cdot 10^{-4}$ , while the LR model stagnates due to the lack of nonlinearity in the input data, reaching only  $\text{NMSE}(\text{LR}) = 7.38 \cdot 10^{-4}$ . QRC, on the other hand, exhibits errors roughly one order of magnitude larger than TD-QELM, with  $\text{NMSE}(\text{QRC}) = 1.59 \cdot 10^{-3}$ . This limitation arises from constant input overwriting, which prevents the system from accessing distant past inputs and performing the nonlinear operations required for the NARMA10 task.

Overall, these results suggest that, although TD-QELM has a restricted memory due to the encoding window, this limitation actually induces rich nonlinear features in the readout, thereby enhancing overall task performance, consistent with the findings reported in [30].

Next, we investigate both the QRC and TD-QELM protocols on actual quantum hardware, with a particular focus on noise accumulation. To this end, we examine how the input length affects the prediction performance of TD-QELM and QRC under three different conditions: (i) ideal noise-free simulation ( $\gamma = 0$ ), (ii) simulation using the hardware-noise model **FakeKawasaki** from the Qiskit package, and (iii) execution on the NISQ device *ibm.kawasaki*, based on IBM’s 127-qubit Eagle superconducting processor. The input length was varied from  $M = 100$  to  $M = 1000$  timesteps in increments of 100. In QRC, repeated re-initialization of the time series results in a computational cost that scales quadratically

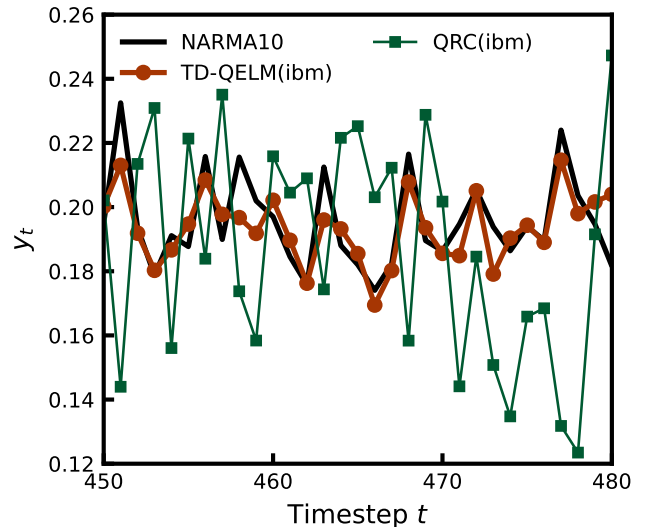


FIG. 4. Time-series output for the NARMA10 task obtained on the *ibm.kawasaki* quantum hardware. The black curve shows the target signal (NARMA10), while the orange and green curves correspond to the outputs of TD-QELM (ibm) and QRC (ibm), respectively.

with the input length  $M$  (see Eq. (6)). This quadratic overhead results in increased circuit depth on quantum hardware, making the system more susceptible to decoherence and gate errors [9]. To test the influence of noise accumulation due to decoherence and gate errors, we adopt a simple QRC architecture without time multiplexing ( $N_V = 1$ ).

As before, the initial 10% of each sequence was used for washout, 70% for training, and 20% for testing. Each circuit was executed with  $N_{\text{shots}} = 8192$ . Under these conditions, QRC could be executed up to 300 timesteps in simulation with **FakeKawasaki** and up to 500 timesteps on the real device (*ibm.kawasaki*), due to computational resource limitations.

Figure 3 illustrates the relationship between input length and prediction performance for TD-QELM (orange) and QRC (green) under different environments. In the noiseless simulation, both TD-QELM (light orange) and QRC (light green) remain largely constant with respect to input length. However, when executed on real IBM quantum devices, QRC’s NMSE (dark green) increases substantially for longer inputs. This behavior is mainly attributed to the repeated re-initialization of the full time series, which increases the total number of circuit executions. In the presence of noise on current quantum hardware, this results in performance degradation, as evidenced by the significantly increased NMSE for  $M > 400$ . TD-QELM (dark orange), in contrast, maintains stable performance with respect to the input length  $M$ , since each input requires the same number of quantum circuits. This behavior is also accurately reproduced by the **FakeKawasaki** noise model.

Table II summarizes the average NMSE values corre-

TABLE II. Average NMSE of TD-QELM and QRC under different environments with varying input lengths. Each value represents the mean over 10 trials. The smallest NMSE value for each timestep is highlighted in bold.

Input length $M$	TD-QELM			QRC		
	Aer(Noiseless)	FakeKawasaki	<i>ibm.kawasaki</i>	Aer(Noiseless)	FakeKawasaki	<i>ibm.kawasaki</i>
100	$2.56 \cdot 10^{-3}$	$1.19 \cdot 10^{-3}$	<b><math>8.61 \cdot 10^{-4}</math></b>	$3.05 \cdot 10^{-3}$	$3.57 \cdot 10^{-3}$	$3.53 \cdot 10^{-3}$
300	$2.46 \cdot 10^{-3}$	$1.30 \cdot 10^{-3}$	<b><math>1.08 \cdot 10^{-3}</math></b>	$4.23 \cdot 10^{-3}$	$4.37 \cdot 10^{-3}$	$4.35 \cdot 10^{-3}$
500	$3.05 \cdot 10^{-3}$	$1.71 \cdot 10^{-3}$	<b><math>1.58 \cdot 10^{-3}</math></b>	$4.51 \cdot 10^{-3}$	–	$8.61 \cdot 10^{-3}$
1000	$1.72 \cdot 10^{-3}$	$1.05 \cdot 10^{-3}$	<b><math>8.81 \cdot 10^{-4}</math></b>	$3.32 \cdot 10^{-3}$	–	–

sponding to Fig. 3 (see Appendix B for the standard deviations). The lowest NMSE for all input lengths and environments is obtained when TD-QELM is implemented on the real device. Here, FakeKawasaki and *ibm.kawasaki* exhibit comparable behavior, with *ibm.kawasaki* outperforming both the noisy simulation and the noiseless TD-QELM case. This noise-enhanced performance has been observed in several QRC studies, where intrinsic hardware noise can positively impact prediction accuracy [10, 24, 26, 28]. In the case of TD-QELM, this implies that natural quantum noise present on NISQ devices can play a constructive role in improving predictive accuracy, underscoring the potential of noise-assisted quantum machine learning. To illustrate the qualitative prediction behavior, Figure 4 shows a segment of the predicted NARMA10 waveform for a given input sequence. Comparison with the NARMA10 target sequence (black) reveals that QRC (dark green) fails to capture the task dynamics, whereas TD-QELM (dark orange), even with a limited readout dimension, closely follows the fluctuations and temporal structure of the target. These results suggest that the repeated re-initialization of the full time series in QRC increases the total number of circuit executions, leading to effective noise accumulation and making QRC challenging to implement on current NISQ hardware. In contrast, TD-QELM not only exhibits increased robustness to noise but also achieves improved task performance, which can be attributed to its ability to map fewer data points onto highly nonlinear features.

*Conclusion.* This work examined limitations of quantum reservoir computing (QRC), particularly noise accumulation and the quadratic scaling of computational cost with input sequence length. To address these issues, we introduced the *time-delayed quantum extreme learning machine* (TD-QELM), which enables parallel encoding of past inputs and reduces the time complexity to linear while improving task performance.

We first considered a transverse-field Ising model with all-to-all connectivity and implemented the reservoir evolution using a single-step Trotterization, resulting in shallow circuits suitable for noisy intermediate-scale quantum (NISQ) devices. Simulations, showed that TD-QELM consistently outperforms conventional QRC in task performance on the NARMA10 task, which is due to the rich non-linear features exhibited by restricted memory, also observed in [30].

To validate these findings under realistic conditions, we conducted simulations with FakeKawasaki and performed experiments on the *ibm.kawasaki* quantum processor. The hardware topology required Hamiltonians tailored to the native qubit connectivity, enabling the design of hardware-constrained quantum reservoirs. Across noiseless simulations, noisy simulations, and hardware execution, TD-QELM outperforms QRC in the NARMA10 task. The need to re-initialize the full time series on current noisy quantum circuits leads to noise accumulation, making QRC difficult to scale. TD-QELM, on the other hand, maintains stable performance for longer sequences due to its shallow-circuit design, reduced operation count, and linear scaling. When considering realistic hardware, TD-QELM performs better in the presence of noise than under noiseless conditions, consistent with previously reported noise-assisted reservoir behavior [10, 24, 26, 28].

Overall, this work demonstrates TD-QELM as a scalable and hardware-efficient alternative to conventional QRC. By mitigating noise accumulation, improving prediction accuracy, and remaining compatible with NISQ devices, TD-QELM provides a promising pathway toward practical quantum time-series processing.

*Acknowledgements.* The authors would like to express their sincere gratitude to Dr. Atsushi Matsuo and Mr. Toru Imai of IBM Japan for their invaluable discussions and constructive suggestions.

[1] M. A. Nielsen, M. R. Dowling, M. Gu, and A. C. Doherty, Quantum Computation as Geometry, *Science* **311**, 1133 (2006).  
 [2] M. AbuGhanem, IBM quantum computers: evolution, performance, and future directions, *J. Supercomput* **81**, 687 (2025).

[3] J. Preskill, Quantum Computing in the NISQ era and beyond, *Quantum* **2**, 79 (2018).  
 [4] F. Arute, K. Arya, R. Babbush, D. Bacon, J. C. Bardin, R. Barends, R. Biswas, S. Boixo, F. G. S. L. Brandão, D. A. Buell, B. Burkett, Y. Chen, Z. Chen, B. Chiaro, R. Collins, W. Courtney, A. Dunsworth, E. Farhi,

- B. Foxen, A. Fowler, *et al.*, Quantum supremacy using a programmable superconducting processor, *Nature* **574**, 505 (2019).
- [5] M. Schuld, I. Sinayskiy, and F. Petruccione, An introduction to quantum machine learning, *Contemp. Phys.* **56**, 172 (2015).
- [6] J. Biamonte, P. Wittek, N. Pancotti, P. Rebentrost, N. Wiebe, and S. Lloyd, Quantum machine learning, *Nature* **549**, 195 (2017).
- [7] M. Cerezo, G. Verdon, H. Huang, L. Cincio, and P. J. Coles, Challenges and opportunities in quantum machine learning, *Nat. Comput. Sci.* **2**, 567 (2022).
- [8] K. Fujii and K. Nakajima, Harnessing disordered-ensemble quantum dynamics for machine learning, *Phys. Rev. Applied* **8**, 024030 (2017).
- [9] J. Chen, H. I. Nurdin, and N. Yamamoto, Temporal information processing on noisy quantum computers, *Phys. Rev. Applied* **14**, 024065 (2020).
- [10] Y. Suzuki, Q. Gao, K. C. Pradel, K. Yasuoka, and N. Yamamoto, Natural quantum reservoir computing for temporal information processing, *Sci. Rep.* **12**, 1353 (2022).
- [11] K. Nakajima, K. Fujii, M. Negoro, K. Mitarai, and M. Kitagawa, Boosting computational power through spatial multiplexing in quantum reservoir computing, *Phys. Rev. Applied* **11**, 034021 (2019).
- [12] J. Garcia-Beni, G. L. Giorgi, M. C. Soriano, and R. Zambrini, Scalable photonic platform for real-time quantum reservoir computing, *Phys. Rev. Applied* **20**, 014051 (2023).
- [13] P. Mujal, R. Martínez-Peña, J. Nokkala, J. Garcia-Beni, G. L. Giorgi, M. C. Soriano, and R. Zambrini, Opportunities in quantum reservoir computing and extreme learning machines, *Adv. Quantum Technol.* **4**, 2100027 (2021).
- [14] A. H. Abbas, H. Abdel-Ghani, and I. S. Maksymov, Classical and quantum physical reservoir computing for on-board artificial intelligence systems: a perspective, *Dynamics* **4**, 643 (2024).
- [15] K. Fujii and K. Nakajima, Quantum reservoir computing: a reservoir approach toward quantum machine learning on near-term quantum devices, in *Reservoir Computing: Theory, Physical Implementations, and Applications*, edited by K. Nakajima and I. Fischer (Springer Singapore, Singapore, 2021) pp. 423–450.
- [16] K. Nakajima, Physical reservoir computing—an introductory perspective, *Jpn. J. Appl. Phys.* **59**, 060501 (2020).
- [17] P. Pfeffer, F. Heyder, and J. Schumacher, Reduced-order modeling of two-dimensional turbulent rayleigh-bénard flow by hybrid quantum-classical reservoir computing, *Phys. Rev. Research* **5**, 043242 (2023).
- [18] N. Götting, S. Wilksen, A. Steinhoff, F. Lohof, and C. Gies, Connection between memory performance and optical absorption in quantum reservoir computing, *Phys. Rev. Lett.* **135**, 240403 (2025).
- [19] M. Vetrano, G. Lo Monaco, L. Innocenti, S. Lorenzo, and G. M. Palma, State estimation with quantum extreme learning machines beyond the scrambling time, *npj Quantum Inf* **11**, 1 (2025).
- [20] R. Martínez-Peña, G. L. Giorgi, J. Nokkala, M. C. Soriano, and R. Zambrini, Dynamical phase transitions in quantum reservoir computing, *Phys. Rev. Lett.* **127**, 100502 (2021).
- [21] K. Kobayashi and Y. Motome, Edge of many-body quantum chaos in quantum reservoir computing, *Phys. Rev. Lett.* **136**, 040602 (2026).
- [22] S. Čindrak, K. Lüdige, and L. C. Jaurigue, From krylov complexity to observability: Capturing phase space dimension with applications in quantum reservoir computing, *Phys. Rev. Research* **7**, L042039 (2025).
- [23] S. Čindrak, L. C. Jaurigue, and K. Lüdige, Engineering quantum reservoirs through krylov complexity, expressivity, and observability, *Phys. Rev. Research* **7**, 043190 (2025).
- [24] T. Kubota, Y. Suzuki, S. Kobayashi, Q. H. Tran, N. Yamamoto, and K. Nakajima, Temporal information processing induced by quantum noise, *Phys. Rev. Research* **5**, 023057 (2023).
- [25] L. Domingo, G. Carlo, and F. Borondo, Taking advantage of noise in quantum reservoir computing, *Sci. Rep.* **13**, 8790 (2023).
- [26] A. Sannia, R. Martínez-Peña, M. C. Soriano, G. L. Giorgi, and R. Zambrini, Dissipation as a resource for Quantum Reservoir Computing, *Quantum* **8**, 1291 (2024).
- [27] F. Monzani, E. Ricci, L. Nigro, and E. Prati, Non-unital noise in a superconducting quantum computer as a computational resource for reservoir computing, [arXiv:2409.07886](https://arxiv.org/abs/2409.07886) (2025).
- [28] G. Franceschetto, M. Płodzień, M. Lewenstein, A. Acín, and P. Mujal, Harnessing quantum back-action for time-series processing, [arXiv:2411.03979](https://arxiv.org/abs/2411.03979) (2024).
- [29] D. Fry, A. Deshmukh, S. Y. Chen, V. Rastunkov, and V. Markov, Optimizing quantum noise-induced reservoir computing for nonlinear and chaotic time series prediction, *Sci. Rep.* **13**, 19326 (2023).
- [30] S. Čindrak, B. Donvil, K. Lüdige, and L. C. Jaurigue, Enhancing the performance of quantum reservoir computing and solving the time-complexity problem by artificial memory restriction, *Phys. Rev. Research* **6**, 013051 (2024).
- [31] T. Yasuda, Y. Suzuki, T. Kubota, K. Nakajima, Q. Gao, W. Zhang, S. Shimono, H. I. Nurdin, and N. Yamamoto, Quantum reservoir computing with repeated measurements on superconducting devices, [arXiv:2310.06706](https://arxiv.org/abs/2310.06706) (2023).
- [32] F. Hu, S. A. Khan, N. T. Bronn, G. Angelatos, G. E. Rowlands, G. J. Ribeill, and H. E. Türeci, Overcoming the coherence time barrier in quantum machine learning on temporal data, *Nat. Commun.* **15**, 7491 (2024).
- [33] P. Mujal, R. Martínez-Peña, G. L. Giorgi, M. C. Soriano, and R. Zambrini, Time-series quantum reservoir computing with weak and projective measurements, *npj Quantum Inf* **9**, 16 (2023).
- [34] K. Kobayashi, K. Fujii, and N. Yamamoto, Feedback-driven quantum reservoir computing for time-series analysis, *PRX Quantum* **5**, 040325 (2024).
- [35] P. Pfeffer, F. Heyder, and J. Schumacher, Hybrid quantum-classical reservoir computing of thermal convection flow, *Phys. Rev. Research* **4**, 033176 (2022).
- [36] J. B. Butcher, D. Verstraeten, B. Schrauwen, C. R. Day, and P. W. Haycock, Reservoir computing and extreme learning machines for non-linear time-series data analysis, *Neural Netw.* **38**, 76 (2013).
- [37] L. Innocenti, S. Lorenzo, I. Palmisano, A. Ferraro, M. Paternostro, and G. M. Palma, Potential and limitations of quantum extreme learning machines, *Commun. Phys.* **6**, 1 (2023).

- [38] A. De Lorenzis, M. P. Casado, M. P. Estarellas, N. Lo Gullo, T. Lux, F. Plastina, A. Riera, and J. Settimo, Harnessing quantum extreme learning machines for image classification, *Phys. Rev. Applied* **23**, 044024 (2025).
- [39] W. Xiong, G. Facelli, M. Sahebi, O. Agnel, T. Chotibut, S. Thanasilp, and Z. Holmes, On fundamental aspects of quantum extreme learning machines, [arXiv:2312.15124](https://arxiv.org/abs/2312.15124) (2023).
- [40] IBM, IBM Quantum Platform, <https://quantum-computing.ibm.com/>.
- [41] T. Kubota, H. Takahashi, and K. Nakajima, Unifying framework for information processing in stochastically driven dynamical systems, *Phys. Rev. Research* **3**, 043135 (2021).
- [42] J. Dambre, D. Verstraeten, B. Schrauwen, and S. Massar, Information processing capacity of dynamical systems, *Sci. Rep.* **2**, 514 (2012).
- [43] J. Lin, F. L. Chung, and S. Wang, A fast parametric and structural transfer leaky integrator echo state network for reservoir computing, *IEEE Trans. Syst. Man Cybern. Syst.* **54**, 3257 (2024).
- [44] E. Picco, L. C. Jaurigue, K. Lüdge, and S. Massar, Efficient optimisation of physical reservoir computers using only a delayed input, *Commun. Eng.* **4**, 3 (2025).
- [45] D. Owen-Newns, L. C. Jaurigue, J. Robertson, A. Adair, J. A. Jaurigue, K. Lüdge, and A. Hurtado, Photonic spiking neural network built with a single vcsel for high-speed time series prediction, *Commun. Phys.* **8**, 110 (2025).
- [46] A. Kandala, A. Mezzacapo, K. Temme, M. Takita, M. Brink, J. M. Chow, and J. M. Gambetta, Hardware-efficient variational quantum eigensolver for small molecules and quantum magnets, *Nature* **549**, 242 (2017).
- [47] M. N. Ivaki, A. Lazarides, and T. Ala-Nissila, Quantum reservoir computing on random regular graphs, *Phys. Rev. A* **112**, 012622 (2025).

## Appendix A: Relationship between error definitions

In this appendix, we derive the relationship between the signal-energy normalized NMSE commonly used in quantum reservoir computing and the variance-normalized NMSE frequently employed in machine learning. The derivation makes explicit how the two error measures differ due to the contribution of the mean (DC component) of the target signal.

$$\begin{aligned} \text{NMSE} &= \frac{\sum_{t=1}^T (y_t - y_t^{\text{target}})^2}{\sum_{t=1}^T (y_t^{\text{target}})^2} \\ \text{NMSE}_{\text{var}} &= \frac{\sum_{t=1}^T (\hat{y}_t - y_t)^2}{\sum_{t=1}^T (y_t - \mathbb{E}[\mathbf{y}])^2}, \end{aligned} \quad (\text{A1})$$

We start from the variance-normalized definition and multiply by unity:

$$\begin{aligned} \text{NMSE}_{\text{var}} &= \text{NMSE}_{\text{var}} \frac{\sum_{t=1}^T y_t^2}{\sum_{t=1}^T y_t^2} \\ &= \text{NMSE} \frac{\sum_{t=1}^T y_t^2}{\sum_{t=1}^T (y_t - \mathbb{E}[\mathbf{y}])^2}. \end{aligned} \quad (\text{A2})$$

To relate the denominators, we use the identity

$$\begin{aligned} \sum_{t=1}^T (y_t - \mathbb{E}[\mathbf{y}])^2 &= \sum_{t=1}^T y_t^2 - 2\mathbb{E}[\mathbf{y}] \sum_{t=1}^T y_t + T\mathbb{E}[\mathbf{y}]^2 \\ &= \sum_{t=1}^T y_t^2 - 2T\mathbb{E}[\mathbf{y}]^2 + T\mathbb{E}[\mathbf{y}]^2 \\ &= \sum_{t=1}^T y_t^2 - T\mathbb{E}[\mathbf{y}]^2, \end{aligned} \quad (\text{A3})$$

which can be rearranged as

$$\sum_{t=1}^T y_t^2 = \sum_{t=1}^T (y_t - \mathbb{E}[\mathbf{y}])^2 + T\mathbb{E}[\mathbf{y}]^2. \quad (\text{A4})$$

Substituting this expression back yields

$$\begin{aligned} \text{NMSE}_{\text{var}} &= \text{NMSE} \frac{\sum_{t=1}^T (y_t - \mathbb{E}[\mathbf{y}])^2 + T\mathbb{E}[\mathbf{y}]^2}{\sum_{t=1}^T (y_t - \mathbb{E}[\mathbf{y}])^2} \\ &= \text{NMSE} \left( 1 + \frac{\mathbb{E}[\mathbf{y}]^2}{\frac{1}{T} \sum_{t=1}^T (y_t - \mathbb{E}[\mathbf{y}])^2} \right) \\ &= \text{NMSE} \left( 1 + \frac{\mathbb{E}[\mathbf{y}]^2}{\text{var}[\mathbf{y}]} \right). \end{aligned} \quad (\text{A5})$$

## Appendix B: Standard deviation of NMSE over repeated trials

In this appendix, we quantify the variability of the NMSE values reported in Table II by evaluating the standard deviation over independent trials. The standard deviation of the NMSE is calculated as

$$\sigma_{\text{NMSE}} = \sqrt{\frac{1}{N-1} \sum_{i=1}^N (\text{NMSE}_i - \overline{\text{NMSE}})^2}, \quad (\text{B1})$$

where  $\text{NMSE}_i$  denotes the NMSE obtained in the  $i$ th independent trials,  $\overline{\text{NMSE}}$  is the mean NMSE over  $N$  trial, and  $N = 10$ . Table III summarizes the standard deviation of the NMSE values evaluated over independent trials. In particular, for the experimental results obtained on quantum hardware, TD-QELM exhibits smaller standard deviations than QRC, indicating more stable and invariant prediction performance with respect to variations in the initial conditions.

TABLE III. Standard deviation of NMSE of TD-QELM and QRC under different environments with varying input length. Each value represents the standard deviation over 10 independent trials. Boldface indicates the smallest standard deviation for each input length.

Input length $M$	TD-QELM			QRC		
	Aer(Noiseless)	FakeKawasaki	<i>ibm_kawasaki</i>	Aer(Noiseless)	FakeKawasaki	<i>ibm_kawasaki</i>
100	$1.48 \cdot 10^{-3}$	$2.86 \cdot 10^{-4}$	<b><math>2.85 \cdot 10^{-4}</math></b>	$3.68 \cdot 10^{-4}$	$7.74 \cdot 10^{-4}$	$6.30 \cdot 10^{-4}$
300	$7.30 \cdot 10^{-4}$	$3.33 \cdot 10^{-4}$	$2.18 \cdot 10^{-4}$	<b><math>1.25 \cdot 10^{-4}</math></b>	$2.78 \cdot 10^{-4}$	$3.32 \cdot 10^{-4}$
500	$8.46 \cdot 10^{-4}$	$2.41 \cdot 10^{-4}$	$2.79 \cdot 10^{-4}$	<b><math>7.67 \cdot 10^{-5}</math></b>	–	$3.36 \cdot 10^{-3}$
1000	$5.55 \cdot 10^{-4}$	$2.11 \cdot 10^{-4}$	$1.39 \cdot 10^{-4}$	<b><math>1.21 \cdot 10^{-5}</math></b>	–	–